# Thin Films of Conductive ZnO Patterned by Micromolding Resulting in Nearly Isolated Features

Ole F. Göbel, Dave H. A. Blank, and Johan E. ten Elshof*

Inorganic Materials Science, Mesa+ Institute for Nanotechnology, University of Twente, P.O. Box 217, 7500 AE Enschede, The Netherlands

**ABSTRACT** Patterned and continuous thin films of conductive Al-doped zinc oxide (ZnO:Al) were prepared on different substrates from a polymeric precursor solution. Their electric conductivity and light transmittance (for visible and UV light) was measured at room temperature. By means of a simple device, conductive ZnO:Al films with high fidelity patterns with features of 2−20 $\mu$m width could be obtained by simply micromolding the liquid precursor film prior to heat treatment. The individual features were interconnected by a very thin residual ZnO layer.

**KEYWORDS:** soft lithography • PDMS • zinc oxide • patterns • thin films.

## 1. INTRODUCTION

Thin films of functional oxides can be patterned in many ways, but for large scale production it is desirable to apply a rather simple yet low-cost technique, provided that the patterning technique produces patterns of sufficient quality. Soft-lithographic patterning techniques can be simple and cheap, but are mainly used for the patterning of organic films (1). Their combination with liquid precursor deposition, often of a sol−gel, can yield inorganic patterned films, and a large variety of approaches has been developed in recent years (2). The most common soft-lithographic methods employed for the patterning of oxide thins films are micromolding in capillaries (3−7), microtransfer molding (8−10), and micromolding and nanoimprinting (10−12).

The list of oxides patterned by any of these four methods comprises Pb(Zr,Ti)$O_3$ (4−7, 10), $TiO_2$, $BaTiO_3$ (12), $ZrO_2$ (3, 9), ZnO (11, 12), $SnO_2$ (3, 12), and many more. The smallest features obtained have diameters of approximately 0.2 $\mu$m (11, 12), but are usually 0.5 $\mu$m (7, 9) or more (3, 6) in diameter.

Micromolding in capillaries or microtransfer molding have the potential to yield patterns of high quality and small feature sizes in oxide films, but are usually slow (micromolding in capillaries) or require delicate preparation of the mold (microtransfer molding). Conventional micromolding is both fast and simple, but suffers from the formation of a residual layer of material spreading between the features of the pattern (10, 11). For several applications, for example micropatterned conductive lines, a residue layer between the features would be inacceptable as it would short-circuit the lines. Hampton et al. (12) report the growth of microtransfer

molded anatase films without residue layer, the absence of which was deduced from SEM images. We evaluated our patterned films by an alternative, much faster method (optical microscopy) and also estimated the sensitivity of this method.

In the case of polymer-based precursor solutions as have been used by us both in this work and in earlier work (11), the formation of the residue layer can be ascribed to the high viscosity of the precursor, combined with its good wetting of the polar substrate, often an oxide layer on a Si wafer. When pressing the mold into the precursor solution, excess liquid has to be removed from underneath the protruding parts of the mold, where the residual layer forms. The higher the pressure applied to the mold, the thinner the residual layer will be. As a result of the viscosity and the wetting, it requires a certain minimum pressure to reduce the thickness of the residue layer to below a chosen threshold. We present here a way of micromolding with a poly-(dimethyl siloxane) (PDMS) mold that leads to the formation of an ultrathin residue layer (~10 nm). The concept is demonstrated by the patterning of conductive Al-doped ZnO (ZnO:Al) films. We used a polymeric precursor solution for ZnO:Al as a model system, because ZnO is a simple oxide yet having physical properties that make it interesting for technical applications. After the precursor solution was patterned and partially dried while it was still confined by the PDMS mold, the mold was released and the patterned film was heated to yield a patterned ZnO film.

For the given precursor solution, we measured the viscosity as a function of temperature. We determined the minimum micromolding pressure required to avoid the formation of a thick residue layer for patterns with two different line widths.

To verify that the patterned ZnO still retained its functionality, we measured two fundamental properties, i.e., the electrical conductivity and the optical transmittance, of the
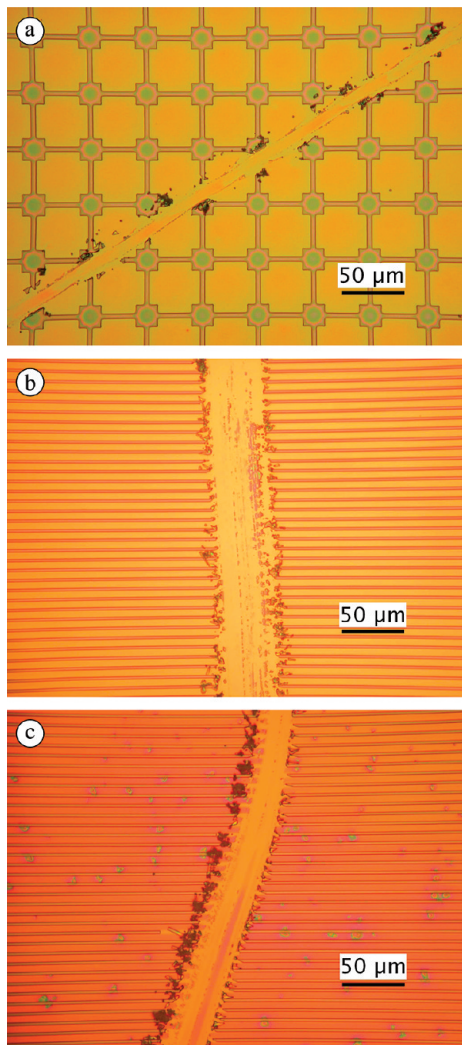
**FIGURE 1. Patterned precursor films (a,b) without and (c) with residue layer between features. All films had been dried at 220 °C. Micromolding conditions: (a) $p = 0.8$ bar, $T = 40$ °C, (b) $p = 1.2$ bar, $T = 30$ °C, (c) $p = 0.2$ bar, $T = 30$ °C. A scratch has been made through all patterns in order to make the color of the substrate visible, so that the presence of a residue layer between the features can be detected.**
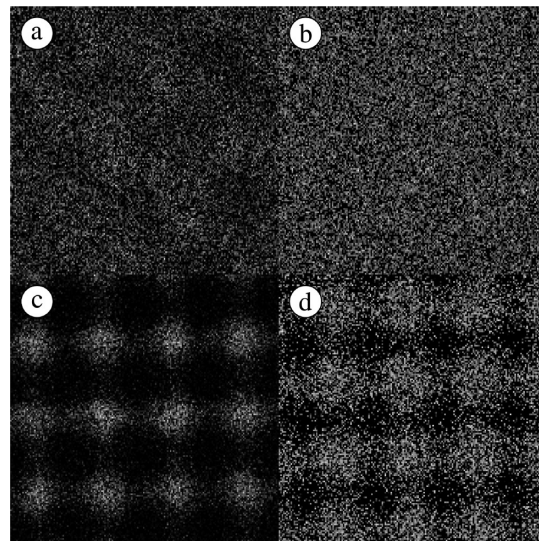


**FIGURE 2. Element concentration maps of a patterned film by XPS (a,b) before sputtering, (c,d) after 2 min Ar sputtering. a and c show the concentration of Zn 3p 3/2 electrons, b and d the concentration of Si 2p electrons. Scan area is $200 \times 200 \ \mu m^2$.**

patterned films. For comparison, we also prepared nonpatterned films from the same precursor solution by the same heating protocol and characterized them, too.

To summarize, we describe here a robust and simple low-cost method to prepare patterned ZnO films consisting of isolated features. The method is believed to be applicable also to many other metal oxides, as preliminary tests on $BiFeO_3$ and $CoFe_2O_4$ suggest. The developed patterning method can thus be useful in the low-cost production of patterned functional oxide films, which could be applied, e.g., as sensors or in data storage. To the best of our knowledge, we present here the first examples of oxide films patterned by soft-lithography which were characterized in terms of technologically interesting properties, at the same time proving that the patterning did not spoil the functionality of the patterned material. We compared these patterned films with nonpatterned ones prepared in a manner as similar as possible to the patterning process.

## 2. EXPERIMENTAL METHODS

**2.1. Chemicals, PDMS, and Substrate Materials.** All chemicals were used as received: $Zn(NO_3)_2 \cdot 6H_2O$, 98% from Aldrich, $Al(NO_3)_3 \cdot 9 H_2O$, 98.5% from Merck, poly(acrylic acid) (PAA), $M_w \approx 2000$, from Aldrich, 2-methoxyethanol, 99.8% from Merck, PDMS type Sylgard 184 from Dow Corning. Substrates were pieces of (100) and (111) oriented Si (Boron-doped) with a grown oxide layer of 400–410 nm thickness, glass microscope coverslips (borosilicate, Roth, Karlsruhe, Germany) and quartz microscope coverslips (UQG Optics Ltd., Cambridge, UK). All substrates were cleaned by snowjetting and exposure to an oxygen plasma immediately before film deposition.

**2.2. Preparation of Precursor Solution.** The precursor solution was made similar to the way described in ref 11: 878 mg of $Zn(NO_3)_2 \cdot 6H_2O$ and 21 mg of $Al(NO_3)_3 \cdot 9 H_2O$ were dissolved in 860 mg of 2-methoxyethanol and 860 mg of water. Then, 900 mg of PAA was added and dissolved, yielding a colorless clear solution.

**2.3. Viscosity.** The dynamic viscosity of the precursor solution was measured on a microviscometer (AMVn-HT, Firmware version 1.70, Anton Paar, Graz, Austria, capillary diameter 1.8 mm, inclination angle 50 and 60°). The density of the solution was determined at 22 °C as 1.298 g/cm$^3$ and expected to remain constant within the temperature range from 20 to 55 °C.

**2.4. PDMS Molds.** PDMS was made according to the guideline of the supplier: Base agent and curing agent were mixed in the weight ratio 10:1 and air bubbles were extracted under vacuum. Afterward, the liquid was cast against a master, a Si wafer with a 1 $\mu$m thick Si oxide layer into which relief patterns had been etched (Lionix B.V., Enschede, The Netherlands). The PDMS was cured at 40 °C overnight, removed from the master, and molds were cut to a size of $1 \times 1$ cm$^2$.

**2.5. Standard Film Deposition.** Continuous films were spincast onto substrates at 2000 rpm for 1 min and subsequently dried on a preheated hotstage at 80 °C for 1 h. Patterned films were obtained by placing approximately 5 $\mu$l of precursor solution on a substrate preheated to the desired deposition temperature. The mold, mounted on a self-built molding machine, was then quickly pressed onto the substrate with the chosen pressure, squeezing out excess precursor solution. While maintaining the pressure, the sample was heated to 80 °C in order to solidify the precursor solution, as
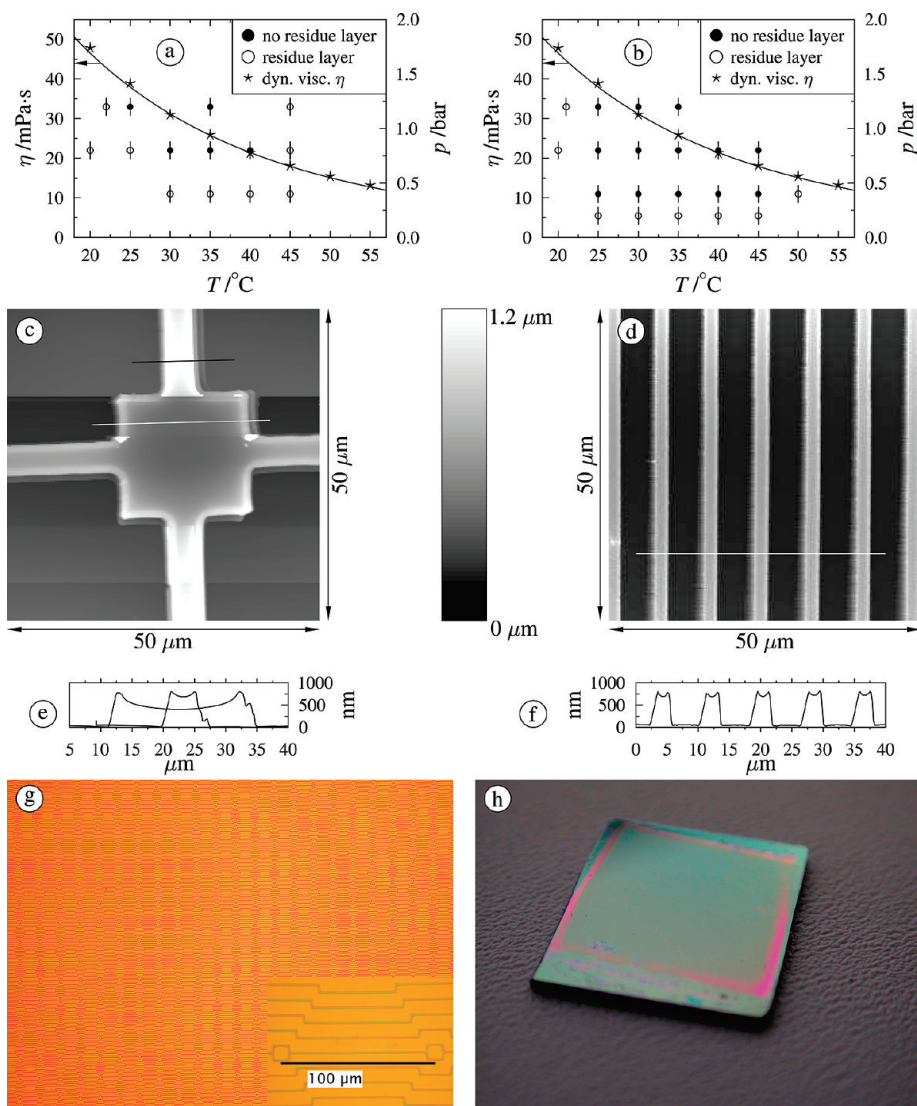
**FIGURE 3.** Viscosity of precursor solution as a function of temperature (stars, line; left axis) and formation of residue layer as a function of temperature and pressure (circles; right axis). Lines of (a) 5 $\mu$m and (b) 2.5 $\mu$m width. Patterned precursor films after drying at 220 °C, scanned by AFM, lines of (c) 5 $\mu$m and (d) 2.5 $\mu$m width, (e, f) corresponding height profiles, (g) another pattern under the optical microscope, (h) the corresponding complete sample with an area of approximately 1 × 1 cm².

2-methoxyethanol diffused into the PDMS. After 30 min, the mold was removed carefully and the sample was kept at 80 °C in air for another 1 h. Afterward, both patterned and unpatterned samples were transferred into a tube furnace preheated to 80 °C and calcined. The heating protocol consisted of five parts: from 80 to 220 °C with 10 °C/min, from 220 to 520 °C with 5 °C/min, from 520 to 620 °C with 10 °C/min, holding at 620 °C for 1 h, and then with −10 °C/min or slower to RT. The lower heating rate between 220 and 520 °C was applied to ensure a smooth degradation of the polymer.

**2.6. Modified Film Deposition.** Patterned films without residual layer could be obtained at molding temperatures of 45 and 50 °C by modifying the process described above. The molds were immersed in 2-methoxyethanol for at least 24 h prior to the experiment in order to fully saturate the PDMS with solvent. Immediately before molding the precursor, the molds were removed from their solvent bath, quickly dried in an air flow and mounted on the molding machine. Then they were lowered into the precursor droplet and left in contact with the solution for several seconds before finally pressing them onto the substrate. This was done to replace the 2-methoxyethanol under the surface of the PDMS mold and give the assumed

viscous precursor layer enough time to dissolve again in the large reservoir of the droplet (see section 3.1).

**2.7. Tempering.** Samples were heated from RT to 400 °C with 10 °C/min, held there, and cooled with the same rate. During the entire tempering process, they were kept in an atmosphere of forming gas (4 vol % $H_2$, 96 vol % $N_2$).

**2.8. X-ray Diffraction, Scanning Electron Microscopy, Atomic Force Microscopy.** The phase purity of the sintered samples was controlled by $\omega - 2\vartheta$-scans carried out on a Philips diffractometer PW3020 (Software XPert Data Collector 2.0e, Panalytical B.V., Almelo, The Netherlands). The topography of unsintered and sintered patterned films was investigated by a JEOL JSM-5610 and a Zeiss LEO-1550 SEM and a Veeco Multimode AFM (tapping mode for unsintered films, contact mode for sintered films).

**2.9. Conductivity.** The sheet resistivity of the films was measured by the Van-der-Pauw method: Four thin copper wires were glued onto the film with silver paste, describing roughly a square of 1 cm². The setup consisted of a Keithley 7001 Switch system, a Keithley 6221 DC and AC Current source, a Keithley 2182A Nanovoltmeter, and a Keithley 2000 Multimeter for monitoring the current.

**2.10. Optical Transparency.** Transmittance spectra of films on glass and quartz microscope coverslips were measured on a dual-beam Cary 50 Scan Spectrometer (Varian, Mulgrave, Victoria, Australia) with air as a standard.

# 3. RESULTS AND DISCUSSION

## 3.1. Patterning.

Patterned precursor films were made according to a standard procedure described in section 2.5. Films with a very thin residue layer of precursor material spreading between the features of the patterns are shown in Figure 1a,b. Figure 1c depicts a sample where a thick residue layer is clearly visible by the color contrast between the scratch (through the pattern) and the voids between the precursor lines. We used optical microscopy (brightfield, Nikon Eclipse ME600) to check for the presence or absence of a thick residual layer, as it is both fast and simple. To estimate the sensitiviy of this detection method, we scanned a patterned film as in Figure 1a by an X-ray photoelectron spectroscopy microscope (Quantera Scanning XPS Microprobe, Physical Electronics, Chanhassen, MN, USA). Initially, the map for Zn 3p 3/2 electrons showed no contrast, indicating that Zn was present everywhere on the sample's surface, see Figure 2 a). Upon sputtering with Ar ions for a short while (1 kV, $2 \times 2$ mm$^2$), a pattern in the Zn map developed as the Zn and O ions were etched away and the residue layer decreased in thickness. A maximum b/w contrast, corresponding to the complete removal of the residue layer, was obtained after etching the quivalent to approximately 10 nm SiO$_2$, see Figure 2c. Also in the Si map, a pattern developed upon sputtering, and reached the maximum contrast together with the pattern of the Zn map. The pattern in the Si map (Figure 2 d) is the negative of the Zn map's pattern, which demonstrates that any spot on the sample is either covered with a thick layer containing Zn, or not covered at all. In other words, the Ar sputtering had fully removed the residue layer.

To avoid the formation of a noticeable residue layer, a minimum pressure $p_{min}$ needs to be applied to the mold. To measure the applied force, we used a self-built device with a force sensor (load cell) mounted between a vertical translation stage and a holder for the PDMS mold. The pressure was calculated from the force and the area of the mold, usually 1 cm$^2$, corrected by the coverage of the particular pattern (i.e., the ratio between protruding area and protruding+receded area). The minimum pressure $p_{min}$ should depend, among others, on the viscosity of the precursor solution. The dynamic viscosity $\eta$ of the precursor solution used in this study varies strongly between 20 and 55 °C, decreasing exponentially with increasing temperature: $\eta(T) = (2.573 \times 10^{-4})\exp(3550/T)$ mPa s ($T$ in K), see Figure 3a,b, stars and full line.

For two specific patterns (1 $\mu$m height in the mold), the presence or absence of a residue layer as a function of molding temperature and pressure was investigated by preparing a number of samples at different conditions. One pattern was a square grid of 5 $\mu$m wide lines, the junctions of which consisted of larger square dots of $20 \times 20$ $\mu$m$^2$, see Figure 1a. The second pattern consisted of parallel lines
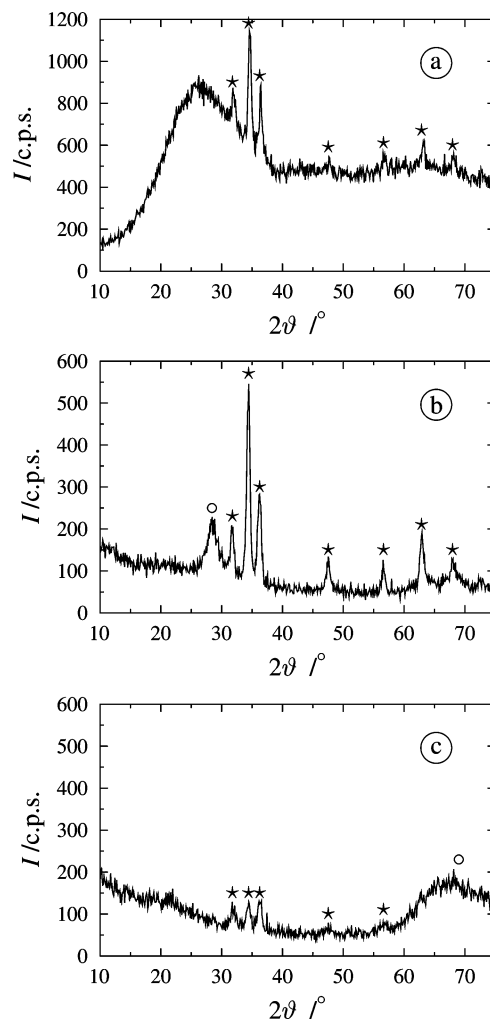
FIGURE 4. XRD $\omega-2\theta$ scans of sintered (600 °C in air) ZnO films: (a) without pattern, not treated after sintering, on glass; (b) without pattern, 4 h at 400 °C in H$_2$/N$_2$ after sintering, on (111)Si/SiO$_2$; (c) patterned, not treated after sintering, on (001)Si/SiO$_2$. Stars denote ZnO peaks, circles denote Si substrate peaks. The scans in b and c were carried out with an offset of 4° in $\omega$ to suppress the peaks of the substrate crystals.

of 2.5 $\mu$m width, see Figure 1b. After drying at 220 °C, all prepared samples were checked for the presence of a residue layer by optical microscopy. The results of these systematic investigations for the two patterns could be plotted in two pseudophase diagrams given in Figure 3a,b, black and white circles. In the case of the first pattern, for lower temperatures, approximately between 25 and 35 °C, $p_{min}$ seems to follow the trend of the viscosity, as far as this can be concluded from the few data points, see Figure 3a. For the second pattern, no dependency of $p_{min}$ on the temperature could be found.

At higher temperatures (45 °C for the pattern with large features, 50 °C for the small feature pattern), we did not succeed in obtaining a pattern without a thick residue layer even at relatively high pressures. The reason for this finding remains unclear. One can assume that at higher temperatures the 2-methoxyethanol diffuses into the PDMS faster that at lower temperatures. The diffusion might lead to the formation of a viscous layer of precursor

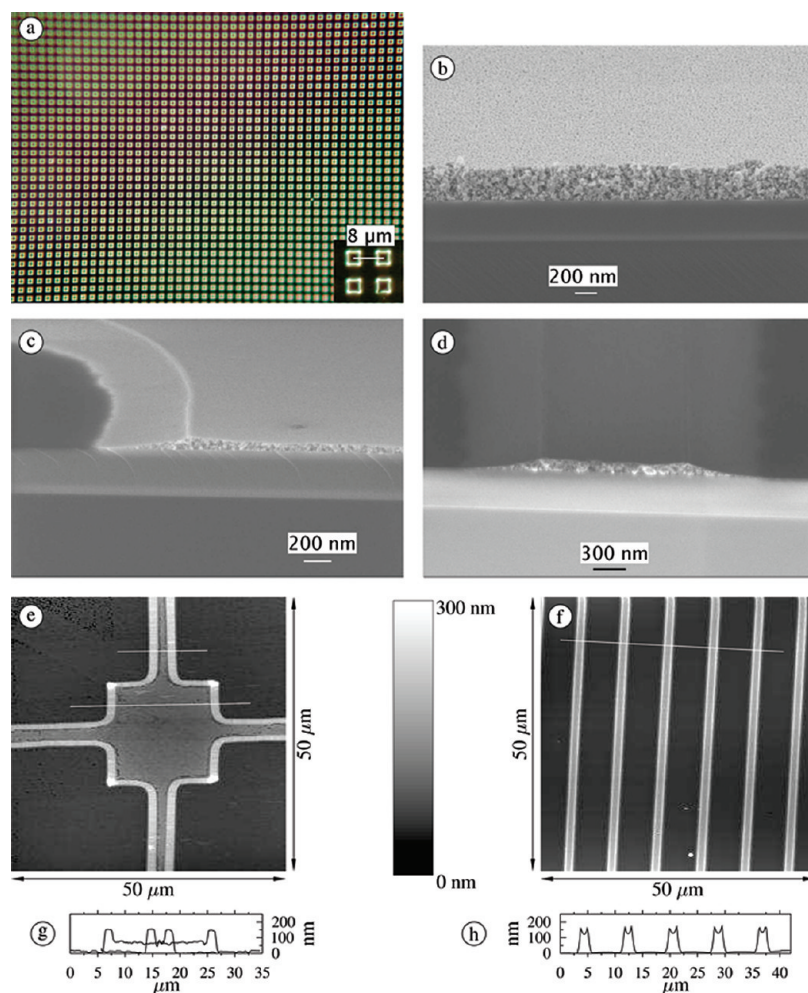 **ACS APPLIED MATERIALS & INTERFACES**

FIGURE 5. Porous ZnO films after pyrolysis. (a) Optical microscope image of a dot-patterned film on glass (dark-field microscopy, glass microscope coverslip bended upon heat treatment). (b) Cross-section SEM image of spin-cast film on Si/SiO$_2$; cross-section SEM image of (c) 5 and (d) 2.5 $\mu$m line-patterned films on Si/SiO$_2$. AFM scans of (e) 5 and (f) 2.5 $\mu$m line-patterned films on Si/ SiO$_2$, with (g, h) corresponding height profiles.

solution covering the PDMS. If this assumed layer is in contact with a sufficiently large reservoir of solution and enough time is provided, it might dissolve again. At higher temperatures, the layer could develop faster than at lower temperatures, and at 45 °C it could develop faster than the time that is required to move the mold from the surface of the precursor droplet down to the surface of the substrate. In this case, the viscous layer would prevent the mold from making contact with the substrate, and would transform into a residue layer. In an attempt to verify this hypothesis, the molding process was slightly modified, as described in Sec. 2.6. The molds were saturated with solvent prior to molding, in order to suppress the formation of the viscous layer. Patterns produced in this manner at 45 and 50 °C showed no residue layer, even when molded with pressures as low as 0.2 bar. This finding thus supports the hypothesis about the formation of the residue layer.

For the pattern with the smaller features, $p_{min}$ appears to be lower than for the larger features pattern, and seems to be independent of the temperature (within the investigated temperature range and with the chosen resolution in pres-

sure), see Figure 3b. The reason for this finding is unclear. However, these two pseudophase diagrams indicate that the patterning process is rather robust in terms of the applied molding parameters ($T$ and $p$). Besides, the pseudophase diagrams can serve as a guide not only to reproduce the two described patterns in ZnO. They could also be used to pattern polymeric precursor solutions for other oxides with patterns similar to the ones investigated in this work, provided that the solutions have similar viscosities and show a similar drying behavior when in contact with PDMS. As an example, we patterned ZnO with bended lines of approximately 1 $\mu$m width (Figure 3g,h) and with tetragonal dots of approximately 4 $\mu$m diameter, see Figure 5a. We also patterned CoFe$_2$O$_4$ and BiFeO$_3$ films without residue layer (not shown). In panels c and d in Figure 3, AFM scans are shown of dried films with the two investigated patterns, whereas panels e and f in Figure 3 show the corresponding height profiles of the two AFM scans. Clearly, a double peak profile has formed in all three features, which has been observed before in patterns of, for example, lead zirconate titanate (4, 6, 7), Sr$_2$Nb$_2$O$_7$ (4), ZrO$_2$ (3), SnO$_2$ (3), and the

formation of which has been explained by Martin and Aksay (6) for the case of sol−gel-derived lead zirconate titanate patterns.

### 3.2. Film Formation and Characterization.
After deposition of the precursor, either by micromolding or by spin-casting, and subsequent drying at 220 °C in air, the films were heated up to degrade the polymer, oxidize the zinc atoms and form a crystalline film of ZnO with zincite crystal structure. The entire pyrolysis was carried out in air and the final temperature was 600 °C, yielding porous films. Figure 4 shows X-ray diffractograms of spin-cast and patterned films. All peaks in the $\omega-2\theta$ scans stemmed from either the substrate or zincite phase ZnO. As revealed by the scanning electron microscope (SEM) images in Figure 5, the porosity of these films is high, making them attractive for possible application in gas sensors. Panels e and f in Figure 3 show the height profiles of films of two patterns, derived from AFM scans, after drying of the films. Panels g and h in Figure 5 show the height profiles of the same patterns, after pyrolysis. These two patterns have three different types of features, i.e., squares of 20 $\mu$m diameter, lines of 5 $\mu$m width, and lines of 2.5 $\mu$m width. The height profiles of three individial features are plotted in Figure 6a−c when applying the mold, after drying, and after pyrolysis. The relative decrease of the features' volumes with respect to the initial volume could be calculated by determining the area under the profile curves, and is shown in Figure 6d. Although the final relative volume is approximately 10 % for all three features, the relative volume after drying of the film is significantly lower in the case of the large square (57 %), compared to the lines (approximately 80 %). The stronger shrinkage of the precursor in the large squares, compared to the lines, mainly takes place in the center of square, away from the edges. This can be seen be comparison of the profiles e and f in Figure 3 and Figure 6a−c. The height of the edges for all three feature types decreases uniformly from 1000 to ca. 800 nm. The central part, however, collapses much more in the large squares, i.e., from 1000 to approximately 400 nm, than in the lines, where the height decreases from 1000 to only approximately 750 nm.

It should be noted that the pattern features remain intact after pyrolysis. Obviously, the adhesion and cohesion of the ZnO phase is good enough to avoid cracking or delamination of the films.

### 3.3. Film Properties.
Films were not conductive after sintering. They could be rendered conductive by applying a tempering step, following a recipe by Schuler and Aegerter (13): Films were heated to 400 °C in forming gas $H_2/N_2$ (4 vol % $H_2$) and held at this temperature for a certain time. To optimize the tempering step, the tempering time of spin-cast films has been varied between 0 and 6 h. All samples on which electrical measurements have been performed had been subjected to this tempering step. The XRD scan of a tempered film is shown in Figure 4b), being nearly identical to that of a nontempered film (not shown). Table 1 lists the sheet resistance of nonpatterned films with different tempering times and of two patterned films. Due to the large
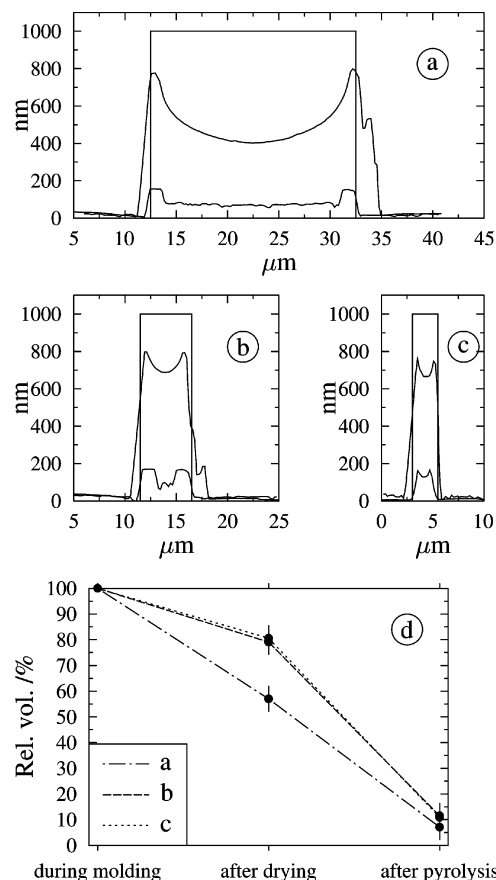


FIGURE 6. Shrinkage of different features during process. Profiles of (a) a square of 20 $\mu$m, (b) a line of 5 $\mu$m, (c) a line of 2.5 $\mu$m diameter. The rectangular profiles were calculated from the known topography of the mold and give the features' profiles during the application of the mold. The curved profiles were derived from AFM scans and depict the profiles after drying the samples and after pyrolysis. d) Relative volumes of the features from (a−c) during micromolding, after drying, and after pyrolysis.

resistivity, Hall measurements failed to give reliable information on the charge carrier type, density, or mobility. Though the measured values of sheet resistance have large errors, they indicate a minimum in resistance for a tempering time of 2 h, in agreement with Schuler (14). The lowest sheet resistance found was $1.99(8) \times 10^5 \Omega/\square$, which is much higher than values reported in literature of 4 $\Omega/\square$ (15). Also the lowest specific resistivity of 8.4(7) $\Omega$ cm is much higher than literature values of, for example, $3.3-3.7 \times 10^{-4}$ $\Omega$ cm (15, 16). The rather high porosity of our films might explain this finding.

The two patterned films in Table 1 have a higher sheet resistance than most of the continuous film, even though they were tempered under optimum conditions. This is clearly due to the lower amount of ZnO:Al per mm$^2$ in the patterned films than in the nonpatterned ones, as the patterns consisted of deep pits in the film. The conduction path in the patterned films is therefore narrower than in the nonpatterned ones, resulting in a higher sheet resistance of the patterned films compared to nonpatterned films tempered under the same conditions.

The visible and UV light transmittance of nonpatterned (spin-cast) and patterned films on glass and quartz micro-

**Table 1. Electrical Properties of Patterned and Nonpatterned Films[a]**

| substrate | pattern | temp time (h) | sheet resistance ($\times 10^5$ $\Omega/\square$) | specific resistivity ($\Omega$ cm) |
|---|---|---|---|---|
| Si/SiO$_2$ | none | 0 | 3.7(3) | 15(1) |
| Si/SiO$_2$ | none | 0.5 | 2.5(2) | 10.0(7) |
| Si/SiO$_2$ | none | 1 | 2.9(3) | 11.6(11) |
| Si/SiO$_2$ | none | 2 | 1.99(8) | 8.4(7) |
| Si/SiO$_2$ | none | 4 | 3.0(1) | 11.8(5) |
| Si/SiO$_2$ | none | 6 | 11.9(2) | 7.8(8) |
| Si/SiO$_2$ | circular holes hex. | 2 | 5.2(3) | |
| Si/SiO$_2$ | circular holes tetr. | 2 | 17.0(3) | |

[a] Resistance measurements were carried out by Van der Pauw method; $I$ was set to 0.01 mA, except for the patterned samples, where $I$ was 0.0030 mA and 0.0015 mA, respectively. Except for the sample with 0 h tempering time and the patterned samples, usually two samples per type were measured and results averaged. The patterns of the two patterned samples are shown in Figure 8.
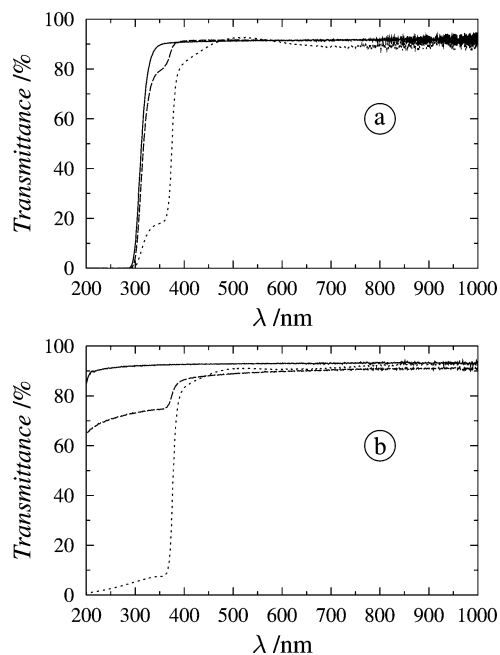


**FIGURE 7. Light transmittance of blank microscope coverslips (full lines), coverslips coated with nonpatterned film (dotted lines), and coverslips with patterned film (dashed lines): (a) glass, (b) quartz microscope coverslips. The transmittance curves of nonheated and heated coverslips without coating were identical, thus the heating-up itself did not affect the transmittance of the substrates.**
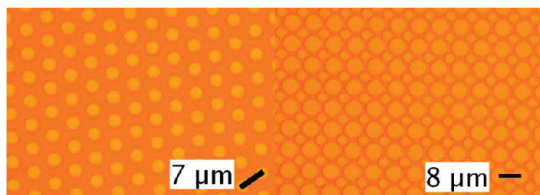


**FIGURE 8. Patterned films on which sheet resistance was measured. Left, circular holes in hexagonal arrangement; right, circular holes in tetragonal arrangement.**

scope coverslips has been measured and results are given in Figure 7. For visible light, the transmittance is not significantly reduced by the continuous coating, as shows the comparison of the full and the dotted lines in Figure 7. Around 520 nm wavelength, in the case of the glass slide, the transmittance even increased, maybe due to a chemical reaction between the boron silicate glass and the ZnO film. The values for the transmittance for visible light amount to ca. 90 %, in good agreement with values reported in litera-

ture (16). For wavelengths below 300 to 360 nm; however, the transmittance is reduced drastically by the continuous film coating (dotted lines). Patterned films (dashed lines), however, reduce the transmittance in the UV range only to a smaller degree than continuous films. This might be exploited to create a pattern in the UV light intensity on the backside of a sample with a patterned coating.

## 4. CONCLUSIONS

By means of the technically simple micromolding technique, patterned films of ZnO:Al have been obtained. The patterns consisted of features (lines, squares) with diameters between 2.5 and 20 $\mu$m, and a height of approximately 100 nm. The micromolding process was carried out at controlled pressure and temperature. Both a temperature and pressure range have been established for two distinct patterns, within which the patterned films will consist of nearly isolated features, interconnected only by a residue layer of less than 15 nm thickness. The patterned films were, upon an additional tempering process, electrically conductive, despite their high porosity. They were also highly transparent for visible light and much less transparent for UV light. Preliminary experiments indicate that the established patterning process is also applicable to other oxides, e.g., CoFe$_2$O$_4$ or BiFeO$_3$.

**REFERENCES AND NOTES**
(1) Xia, Y.; Rogers, J. A.; Paul, K. E.; Whitesides, G. M. *Chem. Rev.* **1999**, *99*, 1823–1848.
(2) ten Elshof, J. E.; Khan, S. U.; Göbel, O. F. *J. Eur. Ceram. Soc.* **2010**, accepted.
(3) Beh, W. S.; Xia, Y.; Qin, D. *J. Mater. Res.* **1999**, *14*, 3995–4003.
(4) Seraji, S.; Wu, Y.; Jewell-Larson, N. E.; Forbess, M. J.; Limmer, S. J.; Chou, T. P.; Cao, G. *Adv. Mater.* **2000**, *12*, 1421–1424.
(5) Martin, C. R.; Aksay, I. A. *J. Mater. Res.* **2005**, *20*, 1995–2003.
(6) Martin, C. R.; Aksay, I. A. *J. Phys. Chem. B* **2003**, *107*, 4261–4268.
(7) Vartuli, J. S.; Özenbaş, M.; Chun, C.-M.; Trau, M.; Aksay, I. A. *J. Mater. Res.* **2003**, *18*, 1259–1265.
(8) Kim, J. H.; Lange, F. F.; Cheon, C. *J. Mater. Res.* **1999**, *14*, 1194–1196.
(9) Moran, P. M.; Lange, F. F. *Appl. Phys. Lett.* **1999**, *74*, 1332–1334.
(10) Khan, S. U.; Göbel, O. F.; Blank, D. H. A.; ten Elshof, J. E. *Appl. Mater. Interfaces* **2009**, *1*, 2250–2255.

(11) Göbel, O. F.; Nedelcu, M.; Steiner, U. *Adv. Funct. Mater.* **2007**, *17*, 1131–1136.

(12) Hampton, M. J.; Williams, S. S.; Zhou, Z.; Nunes, J.; Ko, D.-H.; Templeton, J. L.; Samulski, E. T.; DeSimone, J. M. *Adv. Mater.* **2008**, *20*, 2667–2673.

(13) Schuler, T.; Aegerter, M. A. *Thin Solid Films* **1999**, *351*, 125, 131.

(14) Schuler, T. Ph.D. Thesis, Universität des Saarlandes, Saarbrücken, Germany, 2003.

(15) Hu, J.; Gordon, R. G. *J. Appl. Phys.* **1991**, *71*, 880–890.

(16) Kim, H.; Piqué, A.; Horwitz, J. S.; Murata, H.; Kafafi, Z. H.; Gilmore, C. M.; Chrisey, D. B. *Thin Solid Films* **2000**, *377–378*, 798–802.